IOP Publishing Journal of Physics B: Atomic, Molecular and Optical Physics
J. Phys. B: At. Mol. Opt. Phys. **53** (2020) 075001 (6pp) https://doi.org/10.1088/1361-6455/ab5547

Experimental Stark widths of Mo I and Mo II spectral lines in visible region

Dejan Dojić, Miloš Skočić, Srdjan Bukvić and Stevan Djeniže

University of Belgrade, Faculty of Physics, Studentski Trg 12-16 11000 Belgrade, Serbia

E-mail: ebukvic@ff.bg.ac.rs

Received 9 June 2019, revised 7 October 2019
Accepted for publication 7 November 2019
Published 2 March 2020

Abstract

In the last decade, molybdenum became a very important element for understanding the process of nucleosynthesis. An essential requirement for stellar spectral analysis is the availability of high-quality atomic data, including Stark broadening parameters. In this work we investigate Stark broadening of molybdenum spectral lines from the wavelength range 370 nm–510 nm. This is the first presentation of Stark widths for 18 Mo I and 18 Mo II spectral lines measured at an electron density of $\approx 1.5 \times 10^{23}$ m^{-3} and electron temperature of ≈ 13000 K. Laser induced plasma with well isolated molybdenum spectral lines is employed as a radiation source. Spectra are recorded side-on; the line profiles are obtained via inverse Abel transform. Electron temperature is estimated using the Saha–Boltzmann method. To estimate electron density we applied two techniques. The first is based on the Saha–Boltzmann method for selected Mo I and Mo II spectral lines. In the second approach we rely on the measured width of the well-researched He I 388.86 nm line, as well as on the peak separation of the He I 447.15 nm line. Stark widths normalized to 1×10^{23} m^{-3} electron density are also given. The possible influence of isotope shift and hyperfine structure on spectral line profiles is discussed in detail. Stark shifts of investigated Mo I and Mo II spectral lines, if they exist, are below the detection limit of the experimental setup.

Keywords: atomic data, line profiles, Stark broadening, LIBS

(Some figures may appear in colour only in the online journal)

1. Introduction

Transition probabilities and spectral line broadening parameters are of great importance in diagnostics of remote astrophysical objects and laboratory plasma. While transition probabilities for Mo I are very accurate [1], the number of papers dealing with the broadening of molybdenum lines is relatively small, according to the National Institute of Standards and Technology (NIST) line broadening bibliography [2]. To the knowledge of the authors, Stark broadening of such lines has not yet been measured.

2. Experimental setup

A flat molybdenum sample of high purity (99.9%) was placed inside a home-made chamber filled with helium, at reduced pressure in the range of 0.1–220 mbar. The chamber was mounted on computer controlled x–y–z translation stage to prevent cratering of the sample. The molybdenum sample was illuminated with a powerful (≈ 8 GW cm^{-2} irradiance) laser pulse emitted by a Nd:YAG laser operating at 532 nm. The spatial intensity profile of the laser spot on the target's surface had a top-hat form. Duration of the pulse was 5 ns with a repetition rate of 1 Hz. The optical detection is based on a Andor DH740-18F-03 iStar intensified charge-coupled device (CCD) camera mounted on a McPherson model 209 spectrograph (1.33 m focal length) equipped with a holographic grating of 2400 grooves mm^{-1}. To reduce thermal noise the CCD sensor was cooled down to -20°C. The overall instrumental profile (spectrograph and ICCD camera) can be approximated by the Voigt function with a full width at half-intensity maximum (FWHM) of 8.7 pm measured at 614.3 nm. The image of the plasma is collected side-on and projected onto a 20 μm wide entrance slit with unit magnification, see figure 1.

3. Measurement and diagnostic procedures

The fast expansion is a concomitant features of laser induced plasma (LIP). If LIP is intended for use in line shape investigations it should satisfy certain requirements. Keeping in mind that the image of the plasma is collected side-on, the radial expansion velocity must be sufficiently slow in order to generate negligible small Doppler splitting, i.e. splitting less than the separation between camera pixels [4]. In our experiment this limit is about $3\,\mathrm{km\,s^{-1}}$ for radial expansion velocity. The re-absorbtion of radiation, if present, can distort the shape of the spectral line, so minimal self absorbtion is another important requirement that LIP needs to satisfy. Finally, the electron density of the plasma should produce broadening at least comparable with the instrumental profile width. The basic experimental parameters at which the spectra are recorded: helium pressure, delay time and distance from the sample are chosen to satisfy mentioned requirements. In addition, the amount of helium atoms in the molybdenum plasma was sufficient to provide accurate electron density diagnostics via He I 388.86 nm and 447.15 nm lines. For these experimental parameters and in the wavelength range 370 nm–510 nm, we were able to identify Mo I and Mo II spectral lines. There are no recognized Mo III spectral lines in the range 370nm–510nm in the NIST database [1].

The expansion velocity of the plasma can be controlled efficiently by the surrounding gas type and pressure [5]. Another way to reduce *radial* expansion velocity, keeping the gas pressure relatively low, is to increase size of the laser spot on the target. This arrangement forces plasma expansion in the direction orthogonal to the target surface while the radial expansion remains slow [6]. As a consequence, the spectra collected side-on are less affected by Doppler splitting. The radial expansion velocity can be estimated in straightforward way by comparing the radial size of the emission area for suitable chosen delays. Applying this technique we have verified that expansion velocity of molybdenum atoms and ions, for each pressure/delay/position set of parameters, was below $3\,\mathrm{km\,s^{-1}}$.

It is essential to check that recorded line profiles are free of self-absorbtion. A specific procedure, suitable for LIP, is proposed in [7]. This is basically a sort of 'back mirror' technique developed for cylindrical geometry associated with LIP and spectra recorded in the imaging mode of camera. A simple analytical expression given in [7] provides a way for line profile correction if self absorbtion is small. The optical depth is found to be low, below the detection limit set by noise and other imperfections.

To meet the above-mentioned requirements we have recorded spectra at the distance of 1.6 mm from the molybdenum target, at 220 mbar helium pressure in flowing regime. Delay with respect to the laser trigger was 570 ns while exposure time was set to 30 ns, see [8]. Each spectrum is obtained by averaging images of 50 consecutive laser shots. Shorter exposures (10 ns for example) generate the same spectra; however the number of averaging (and target drilling) is proportionally higher.

Inhomogeneity along the radius is specific to LIP; for this reason use of inverse Abel transform is a necessary step in processing the spectra recorded side-on. An approach proposed in [9] is developed for plasmas with undetermined radius and works well in the case of LIP. Relying on Abel inversion we found that helium spectral lines are very weak in the center of the plasma plume, because helium is pushed to the periphery by molybdenum atoms. A reasonable intensity of helium spectral lines is found for a radial distance of 0.432 mm or higher. At this radius molybdenum lines are also clearly visible, we therefore adopted a radial position of 0.432 mm as a good compromise for electron density diagnostics based on He I lines, as well as for line shape investigation of molybdenum spectral lines.

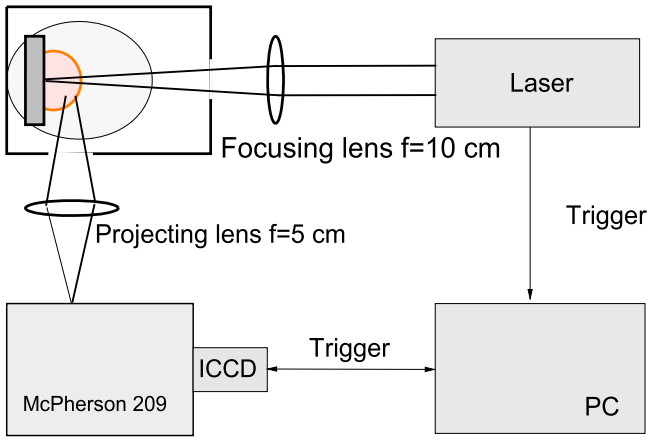

Figure 1. The experimental setup with a simplified drawing of the hot plasma front. The laser output wavelength is 532 nm, and focal length of the focusing lens is 10 cm. Reprinted from [3], copyright (2018), with permission from Elsevier.

4. Electron density and electron temperature measurement

The electron density n_e is estimated applying two different techniques. The first is based on the Saha–Boltzmann method for selected Mo I and Mo II spectral lines. The second relies on well-researched shapes of two He I spectral lines, namely the width of the He I 388.86 nm line and the peak separation of the He I 447.15 nm line. All intensities (He I, Mo I, Mo II) are measured after inverse Abel transform, and all in the region $0.432\,\mathrm{mm} < r < 0.532\,\mathrm{mm}$ and at the distance $x = 1.6\,\mathrm{mm}$ from the target.

4.1. Saha–Boltzmann method

This simple and efficient method is proposed in [10] and re-elaborated in [11]. At the input this method requires relative experimental intensities and transition probabilities for several spectral lines from atomic and ionic ionization states. The method provides two essential quantities—electron temperature and electron density, under the assumption that plasma is in local thermodynamic equilibrium (LTE). The method is not very sensitive in relation to the electron density value, thus, the electron density is always estimated with uncertainty higher than the error reported for the electron temperature. However, sufficiently small errors in the transition probabilities and sufficiently

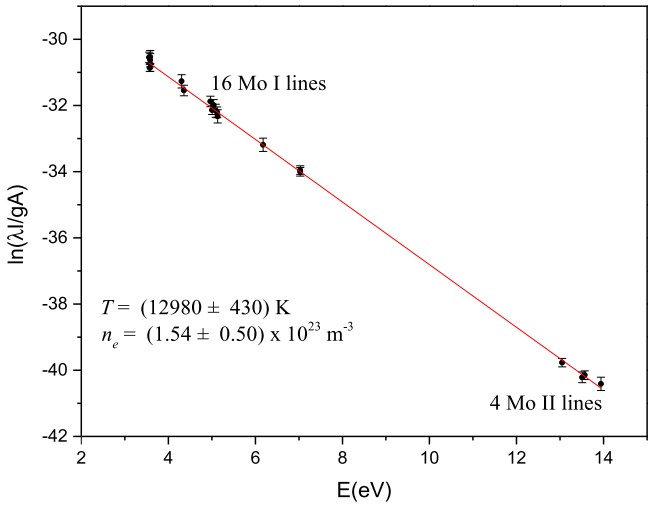

Figure 2. Saha–Boltzmann plot with 16 Mo I lines and 4 Mo II lines.

small errors in the experimental line intensities can result in reasonably accurate value for the electron density. To apply the Saha–Botzmann method we selected 16 Mo I lines and 4 Mo II lines. All the Mo I lines transition probabilities, taken from NIST [1], are with uncertainties of 10% or better (mark B or better). Transition probabilities for the Mo II lines are taken from [12]. The authors report uncertainties of ≈ 10%. The relative experimental intensities are considered to be proportional to the area under the best fit Voigt profile for each spectral line. The errors in the experimental intensities are in the range of 7%–10%.

In figure 2 we present a Saha–Boltzmann plot with individual error bars. A correctly weighted least square algorithm[1] reports the electron temperature value $T_e = (12980 \pm 480)$ K while the electron density is $n_e = (1.54 \pm 0.50) \times 10^{23}\,\mathrm{m}^{-3}$. The electron temperature is mostly defined by the well grouped Mo I lines. The Mo II lines, because of the small energy span with respect to the ionization energy, mainly determine the electron density value. Due to nature of a Saha–Boltzmann plot the electron density and the electron temperature are not independent, they satisfy the Saha equation. According to the condition proposed by McWhirter [13, 14] our plasma was in LTE.

4.2. Electron density estimation relying on He diagnostic lines

According to [15], in the region $n_e > 10^{23}\,\mathrm{m}^{-3}$ there is only one experimental result [16] and a few theoretical predictions for the FWHM of the He I 388.86 nm line. All the results are reasonably consistent. The FWHM of the He I 388.86 nm line in our experiment is estimated to be $w = (0.44 \pm 0.04)$ nm and, according to [16], the corresponding electron density is $n_e \approx 1.5 \times 10^{23}\,\mathrm{m}^{-3}$ which is in good agreement with the results obtained from Saha–Boltzmann plot. Relying on the Born approximation [15], it follows that the same FWHM of 0.44 nm corresponds to the electron density of $n_e \approx 1.77 \times 10^{23}\,\mathrm{m}^{-3}$. The electron density is also estimated relying on the peak separation of the He I 447.15 nm line [17, 18]. The value of $n_e \approx 1.4 \times 10^{23}\,\mathrm{m}^{-3}$ coincides with the above results within 30%, so we adopted for the electron density value of $n_e = (1.54 \pm 0.50) \times 10^{23}\,\mathrm{m}^{-3}$.

[1] Saha–Boltzmann fit is not an option in Origin software. Figure 2 is only a presentation of the fit completed in a custom-made program.

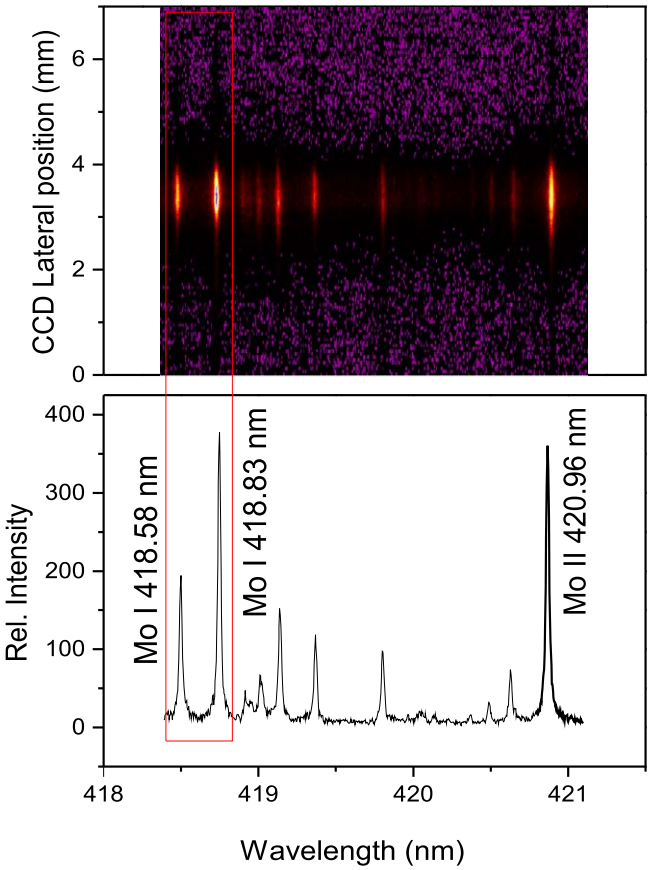

Figure 3. (a) Full CCD frame recorded at 1.6 mm distance from the molybdenum target and delay set to 570 ns. Helium pressure was 220 mbar. (b) Regular spectrum after Abel inversion at $r = 0.432$ mm. Line Mo II 420.96 nm is identified relying on data in reference [19]. The red rectangle indicates the segment of the spectrum shown in figure 3.

5. Data processing procedure

All investigated Mo I and Mo II spectral lines are symmetric with shift, if present, below our detection limit. We applied the following numerical procedure. All spectral lines are recorded side-on in the imaging mode of the CCD camera, see figure 3. Inverse Abel transform [9] is employed to reconstruct line profiles at radial position $0.432\,\mathrm{mm} < r < 0.532\,\mathrm{mm}$ and at distance $x = 1.6$ mm from the target, see figure 4. The Voigt profile is adopted as an appropriate symmetric model function. We suppose that the Gaussian component of the Voigt is due to Doppler and instrumental broadening. It is calculated separately and supplied to the fitting procedure as the fixed value. The Lorentz fraction caused by the Stark effect is obtained after subtracting the Lorentz component, present in the instrumental profile, from the best fit Lorentz parameter of the Voigt model function after applying a nonlinear minimization procedure.

Table 1. Summary of experimental data for Mo I spectral lines. In Column 3 we present our Stark FWHM values (w) of investigated Mo I spectral lines measured at $n_e = 1.54 \times 10^{23}\,\mathrm{m}^{-3}$ and $T_e \approx 13000$ K. The uncertainties in w reported by the least-squares algorithm are typically in the range 0.1 pm–0.15 pm. Taking in account possible systematic errors we have rounded uncertainties to one significant figure, i.e to $\Delta w = 0.2$ pm for all lines. Column 4 contains Stark widths normalized to electron density $n_e = 1 \times 10^{23}\,\mathrm{m}^{-3}$ with uncertainties of 30%. Transitions and corresponding wavelengths are taken from the NIST spectral line database [1].

1 Transition Mo I	2 λ (nm)	3 w (pm) $n_e = 1.54 \times 10^{23}\,\mathrm{m}^{-3}$	4 w_{norm} (pm) $n_e = 10^{23}\,\mathrm{m}^{-3}$
$4d^5 5p\ y\ {}^5F^o_4$ - $4d^5 5s\ a\ {}^5G_5$	406.21	9.6	6.3 ± 1.9
$4d^5 5p\ y\ {}^5F^o_5$ - $4d^5 5s\ a\ {}^5G_6$	406.99	15.8	10.3 ± 3.1
$4d^5 5p\ y\ {}^3I^o_6$ - $4d^5 5s\ a\ {}^3I_5$	418.58	15.1	9.8 ± 2.9
$4d^5 5p\ z\ {}^5H^o_6$ - $4d^5 5s\ a\ {}^5G_5$	418.83	13.2	8.6 ± 2.6
$4d^5 5p\ z\ {}^5H^o_5$ - $4d^5 5s\ a\ {}^5G_4$	423.26	13.1	8.5 ± 2.5
$4d^4 5s5p\ z\ {}^5F^o_4$ - $4d^4 5s^2\ a\ {}^5D_3$	428.86	8.2	5.3 ± 1.6
$4d^4 5s5p\ z\ {}^5F^o_3$ - $4d^4 5s^2\ a\ {}^5D_2$	429.32	9.9	6.4 ± 1.9
$4d^5 5p\ z\ {}^5G^o_4$ - $4d^5 5s\ a\ {}^5G_4$	443.49	18.0	11.7 ± 3.5
$4d^4 5s5p\ y\ {}^5D^o_3$ - $4d^5 5s\ a\ {}^5G_3$	444.97	12.2	7.9 ± 2.4
$4d^5 5p\ z\ {}^5G^o_3$ - $4d^5 5s\ a\ {}^5G_3$	445.74	11.0	7.1 ± 2.1
$4d^5 5p\ z\ {}^3K^o_7$ - $4d^5 5s\ a\ {}^1I_6$	453.68	20.3	13.2 ± 3.9
$4d^4 5s5p\ y\ {}^5P^o_3$ - $4d^4 5s^2\ a\ {}^5D_4$	462.65	14.4	9.4 ± 2.8
$4d^5 5p\ z\ {}^3H^o_4$ - $4d^5 5s\ a\ {}^3G_3$	470.72	22.6	14.7 ± 4.4
$4d^5 5p\ z\ {}^3H^o_5$ - $4d^5 5s\ a\ {}^3G_4$	473.14	21.1	13.7 ± 4.1
$4d^5 5p\ z\ {}^3H^o_6$ - $4d^5 5s\ a\ {}^3G_5$	476.02	25.4	16.5 ± 4.9
$4d^5 5p\ y\ {}^3F^o_4$ - $4d^5 5s\ a\ {}^3G_5$	481.92	16.6	10.8 ± 3.2
$4d^5 5p\ y\ {}^3F^o_3$ - $4d^5 5s\ a\ {}^3G_4$	483.05	20.7	13.5 ± 4.0
$4d^4 5s5p\ y\ {}^5D^o_4$ - $4d^5 5s\ b\ {}^5D_4$	505.99	18.4	11.8 ± 3.6

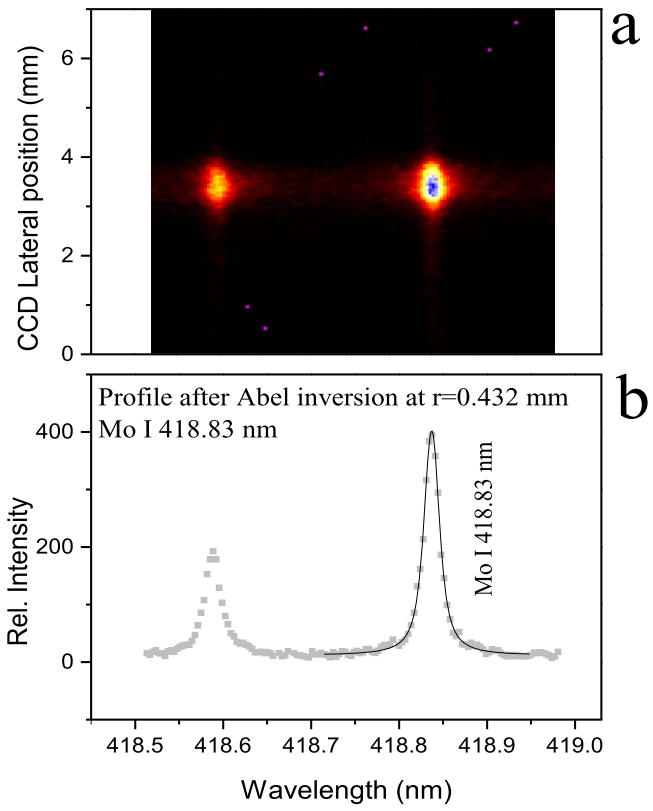

Figure 4. (a) Enlarged segment of the CCD frame with Mo I 418.83 nm line. (b) Gray points are experimental profiles after Abel inversion at $r = 0.432$ mm. Full black line is the best fit to the Voigt profile.

6. Results and discussion

In table 1 we present experimental Stark widths (FWHM) for 18 Mo I lines ranging from 400 nm to 510 nm. Column 3 contains actual data measured at $n_e = 1.54 \times 10^{23}\,\mathrm{m}^{-3}$ electron density and $T_e \approx 13000$ K. Due to the small amount of noise present in the experimental data and sufficient number of data points across the line profiles uncertainties reported by the least-square algorithm are small, between 1.5 pm and 2.5 pm. After reducing to one significant figure we adopted value $\Delta w = 0.2$ pm for all lines. In column 4 we report Stark widths normalized to $n_e = 1 \times 10^{23}\,\mathrm{m}^{-3}$ electron density. The error of ≈ 30%, after normalization, is mainly due to uncertainty present in the electron density.

Stark widths w for 18 Mo II lines in the wavelength interval from 370 nm to 490 nm are presented in table 2. Column 3 contains Stark widths measured at $n_e = 1.54 \times 10^{23}\,\mathrm{m}^{-3}$ electron density and $T_e \approx 13000$ K. In column 4 we present Stark widths w normalized to $n_e = 1 \times 10^{23}\,\mathrm{m}^{-3}$ electron density. As for Mo I, the spectral line errors of ≈ 30% are mainly due to uncertainty in the electron density value. All transitions are taken from [20] except the final one, which is taken from [19].

6.1. Isotope shift and hyperfine structure

Molybdenum has seven stable isotopes ranging from ^{92}Mo to ^{100}Mo. Spectral lines belonging to the same transition, but emitted by different isotopes, are slightly shifted one against the other. Two of these isotopes, ^{95}Mo and ^{97}Mo, have nuclear spin

Table 2. Summary of experimental data for Mo II spectral lines. In Columns 3 we present our Stark FWHM values (w) of investigated Mo II spectral lines measured at $n_e = 1.54 \times 10^{23}$ m^{-3} and $T_e \approx 13000$ K. Uncertainties, reduced to one significant figure, are $\Delta w = 0.2$ pm for all lines. Column 4 contains Stark widths normalized to electron density $n_e = 1 \times 10^{23}$ m^{-3} with 30% uncertainties. Wavelength and transitions are taken from [20], except the last line in the table, where the wavelength is taken from [19].

1	2	3	4
Transition	λ (nm)	w (pm) $n_e = 1.54 \times 10^{23}$ m^{-3}	w_{norm} (pm) $n_e = 10^{23}$ m^{-3}
Mo II			
$4d^4 6p\ z\ {}^4G_{7/2}$ - $4d^4 5s\ b\ {}^2H_{9/2}$	378.21	15.4	10.0 ± 3.0
$4d^4 5p\ z\ {}^4I_{9/2}$ - $4d^4 5s\ b\ {}^2G_{9/2}$	378.32	15.2	9.9 ± 3.0
$4d^4 5p\ z\ {}^2S_{1/2}$ - $4d^4 5s\ a\ {}^2P_{1/2}$	378.64	14.7	9.6 ± 2.9
$4d^4 6p\ z\ {}^6D_{5/2}$ - $4d^4 5s\ b\ {}^4D_{3/2}$	385.72	15.6	10.2 ± 3.0
$4d^4 5p\ z\ {}^4H_{13/2}$ - $4d^4 5s\ b\ {}^2H_{11/2}$	386.13	14.6	9.9 ± 2.8
$4d^4 5p\ z\ {}^6D_{9/2}$ - $4d^4 5s\ b\ {}^4D_{7/2}$	394.15	16.6	10.8 ± 3.2
$4d^4 5p\ z\ {}^6D_{5/2}$ - $4d^4 5s\ b\ {}^4D_{7/2}$	396.15	20.6	13.4 ± 4.0
$4d^4 5p\ z\ {}^6D_{3/2}$ - $4d^4 5s\ b\ {}^4D_{5/2}$	398.62	20.8	13.5 ± 4.0
$4d^4 5p\ z\ {}^6P_{5/2}$ - $4d^4 5s\ b\ {}^4D_{7/2}$	411.96	19.3	12.6 ± 3.8
$4d^4 5p\ z\ {}^2D_{5/2}$ - $4d^4 5s\ c\ {}^2F_{7/2}$	412.23	16.7	10.8 ± 3.3
$4d^4 5p\ z\ {}^4P_{5/2}$ - $4d^4 5s\ b\ {}^4D_{5/2}$	420.96	17.0	11.0 ± 3.3
$4d^4 5p\ z\ {}^2D_{3/2}$ - $4d^4 5s\ c\ {}^2F_{5/2}$	424.47	19.7	12.8 ± 3.8
$4d^4 5p\ z\ {}^4P_{5/2}$ - $4d^4 5s\ b\ {}^4D_{7/2}$	425.07	19.9	13.0 ± 3.9
$4d^4 5p\ z\ {}^4P_{3/2}$ - $4d^4 5s\ b\ {}^4D_{3/2}$	427.90	21.0	13.7 ± 4.1
$4d^4 5p\ z\ {}^4P_{3/2}$ - $4d^4 5s\ b\ {}^4D_{5/2}$	436.36	19.2	12.5 ± 3.7
$4d^4 5p\ z\ {}^4P_{1/2}$ - $4d^4 5s\ b\ {}^4D_{1/2}$	437.78	19.7	12.8 ± 3.8
$4d^4 5p\ z\ {}^4P_{1/2}$ - $4d^4 5s\ b\ {}^4D_{3/2}$	443.35	20.8	13.5 ± 4.0
—	485.36	18.9	12.3 ± 3.7

$I = 5/2$, which introduces hyperfine structure in spectral line profiles [21]. Generally, isotope shift (IS) and hyperfine structure (hfs) affect the profiles of the spectral lines. Whether this influence is visible or not depends on the broadening mechanisms present in the plasma and the magnitude of IS and hfs. For 6 (424.47, 425.06, 427.90, 474.26, 485.36, 420.96 nm) of the 18 Mo II lines investigated in this work the experimental values for IS and hfs are reported in [21]. Relying on these values we were able to check the effect of IS and hfs on the Stark widths for the Mo II lines mentioned. Instead of an approximate experimental profile of the spectral lines with a single Voigt function, we used superposition of seven Voigt functions with centers shifted one against the other according to the IS pattern measured in [21]. The relative intensity of each Voigt is fixed with respect to the intensity of ^{98}Mo, consistent with the relative abundance of molybdenum isotopes. Total splitting due to IS reported in [21] is about 1 pm or less, depending on the spectral line. Splitting introduced by hfs for ^{95}Mo and ^{97}Mo is one order of magnitude smaller, so we approximated the line profiles of these isotopes with a single Voigt function each. Even though the model function is complex, the number of free parameters is only four. It is supposed that the Lorentz component of each Voigt function is the same, as well as the Gauss component. As for the single Voigt, the Gauss component is supposed to be due to Doppler and instrumental broadening, and it is calculated separately and supplied to the fitting procedure as the fixed value. The remaining free parameters are the center and intensity of the ^{98}Mo Voigt function and the baseline common for all profiles.

In table 3 we present the Stark widths for six Mo II lines obtained supposing that the model function is a single Voigt function, column 2, and approximating the model function with a superposition of seven Voigt profiles in accordance with the IS patterns reported in [21], column 3. As is expected the Stark widths are marginally smaller if IS is taken into account, however, the correction is well below the typical uncertainties of Stark widths. We can conclude that Stark broadening is the most dominant process responsible for the shape of Mo II spectral lines and, therefore, the IS and hfs splitting are of marginal influence on electron densities present in the LIP employed in our experiment.

Table 3. Column 2: Stark widths if line profiles are approximated with a single Voigt function. Column 3: Stark widths if line profiles are approximated with a superposition of seven Voigt functions in accordance with the IS patterns reported in [21].

1	2	3	4
λ (nm)	w (pm) Single Voigt	w (pm) IS structure	Δw (pm)
Mo II			
424.47	19.70	19.68	0.2
425.07	19.98	19.92	0.2
427.90	21.04	20.96	0.2
436.36	19.22	19.20	0.2
437.78	19.70	19.62	0.2
443.35	20.80	20.78	0.2

7. Conclusion

In this work we investigate profiles of 18 Mo I and 18 Mo II spectral lines from the wavelength range 370 nm–510 nm, in order to determine Stark broadening parameters at electron

density of $\approx 1.5 \times 10^{23}\,\mathrm{m}^{-3}$ and electron temperature of $\approx$ 13000 K. Laser induced plasma with well isolated molybdenum spectral lines is employed as a radiation source. Spectra are recorded side-on; the line profiles are obtained via inverse Abel transform. Electron temperature is estimated relying on the Saha–Boltzmann method. To estimate electron density we applied two techniques. The first is based on the Saha–Boltzmann method for selected Mo I and Mo II spectral lines. The second approach used the measured width of the well-researched He I 388.86 nm line, as well as the peak separation of the He I 447.15 nm line. The Stark widths of a total of 36 molybdenum spectral lines are presented. Stark widths normalized to $1 \times 10^{23}\,\mathrm{m}^{-3}$ electron density are also given. The possible influence of isotope shift and hyperfine structure on spectral line profiles are discussed in detail. Stark shifts of the investigated Mo I and Mo II spectral lines, if they exist, are below the detection limit of the experimental setup.

Acknowledgments

This work is part of the project 'Determination of atomic parameters on the basis of spectral line profiles' (ON171008), supported by the Ministry of Education and Science of the Republic of Serbia.

ORCID iDs

Srdjan Bukvić https://orcid.org/0000-0002-8202-6225

References

[1] Kramida A, Yu R, Reader J and NIST ASD Team 2019 *NIST Atomic Spectra Database* (Gaithersburg, MD: National Institute of Standards and Technology) (https://physics.nist.gov/asd) (ver. 5.6.1)
[2] Kramida A 2019 *Atomic Spectral Line Broadening Bibliographic Database* (Gaithersburg, MD: National Institute of Standards and Technology) (https://physics.nist.gov/Elevbib) (version 3.0)
[3] Dojic D, Skocic M and Bukvic S 2018 *JQSRT* **207** 73–7
[4] Bukvic S and Skocic M 2017 *Spectrochim. Acta* B **132** 56–60
[5] Jagdish P and Thakur S N 2007 *Laser-Induced Breakdown Spectroscopy* (Amsterdam: Elsevier) 9780080551012
[6] Singh R K and Narayan J 1990 *Phys. Rev* B **41** 8843–61
[7] Burger M, Skocic M and Bukvic S 2014 *Spectrochim. Acta* B **101** 51–6
[8] Aragon C and Aguilera J 2008 *Spectrochim. Acta* B **63** 893–916
[9] Ignjatovic L and Mihajlov A 2002 *JQSRT* **72** 677–89
[10] Yalcin S, Crosley D, Smith G and Faris G 1999 *Appl. Phys.* B **68** 121–30
[11] Aguilera J and Aragon C 2007 *Spectrochim. Acta* B **62** 378–89
[12] Mayo-Garcia R, Aragon C, Aguilera J and Ortiz M 2015 *J. Phys. B: At. Mol. Opt. Phys.* **48** 215002
[13] McWhirter R 1965 *Plasma Diagnostic Techniques* (New York: Academic Press)
[14] Cristoforetti G, De Giacomo A, Dell'Aglio M, Legnaioli S, Tognoni E, Palleschi V and Omenetto N 2010 *Spectrochim. Acta* B **65** 86–95
[15] Omar B, González M A, Gigosos M A, Ramazanov T S, Jelbuldina M C, Dzhumagulova K N, Zammit M, Fursa D and Bray I 2014 *Atoms* **2** 277–98
[16] Berg H, Ali A, Lincke R and Griem H 1962 *Phys. Rev.* **125** 199–206
[17] Barnard A J, Cooper J and Shamey L J 1969 *A&A* **1** 28
[18] Milosavljevic V and Djenize S 2001 *Eur. Phys. J.* D **15** 99–104
[19] Zajdelj A N, Prokofijev V K, Rajskij S M, Slavnij V A and Srejder E Y 1977 *Spectral Lines Tables* (Moscow: Nauka)
[20] Kurucz R and Gell B 1995 *Atomic Line Data Kurucz CD-ROM No. 23* (Cambridge, MA: Smithsonian Astrophysical Observatory)
[21] Rosner S and Holt R 2016 *Can. J. Phys.* **94** 1195–9